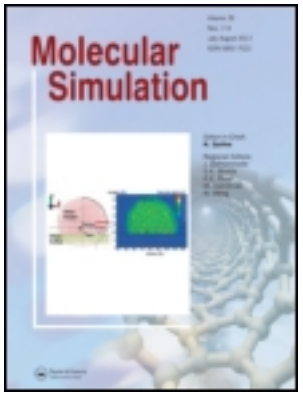

Molecular Simulation
Publication details, including instructions for authors and subscription information:
http://www.tandfonline.com/loi/gmos20

Development of semi-ab initio interionic potential for CaO and MgO

Zhiwei Cui[a], Yi Sun[a] & Jianmin Qu[b]
[a] Department of Astronautic Science and Mechanics, Harbin Institute of Technology, Harbin150001, P.R. China
[b] Department of Mechanical Engineering, Northwestern University, Evanston, IL60208, USA
Published online: 16 Apr 2013.

To cite this article: Zhiwei Cui, Yi Sun & Jianmin Qu (2013) Development of semi-ab initio interionic potential for CaO and MgO, Molecular Simulation, 39:12, 956-967, DOI: 10.1080/08927022.2013.784759

To link to this article: http://dx.doi.org/10.1080/08927022.2013.784759

Molecular Simulation, 2013
Vol. 39, No. 12, 956–967, http://dx.doi.org/10.1080/08927022.2013.784759

Taylor & Francis
Taylor & Francis Group

Development of semi-*ab initio* interionic potential for CaO and MgO

Zhiwei Cui[a], Yi Sun[a]* and Jianmin Qu[b]

[a]*Department of Astronautic Science and Mechanics, Harbin Institute of Technology, Harbin 150001, P.R. China;* [b]*Department of Mechanical Engineering, Northwestern University, Evanston, IL 60208, USA*

(*Received 9 August 2012; final version received 7 March 2013*)

In this paper, we propose a novel method to derive the interionic potentials for CaO and MgO in conjunction with *ab initio* calculation and empirical three-body interaction. By using the Chen–Mobius lattice inversion, the pairwise interaction between cations and anions can be evaluated from multiple virtual structures. The quantum-chemistry calculation is carried out to derive the short-range potential for the same species of ions. Empirical three-body interactions are then adopted to heal the drawbacks arising from purely pairwise potential, such as Cauchy relation. The proposed potential is verified by molecular dynamics simulations of some primary properties, including pressure and temperature dependence of lattice constant, elastic constants and phase transition of CaO and MgO. Simulation results are in good agreement with the existing experimental data and *ab initio* calculations, showing that the developed potentials are valid over a wide range of interionic separations. It is believed that this approach can be readily extended into other materials.

Keywords: *ab initio*; Chen–Mobius lattice inversion; interionic potential; molecular dynamics simulation; elastic constants

1. Introduction

On the basis of the Chen–Mobius inversion [1–3] and quantum chemistry technique [4,5], we have derived the interionic pair potentials of solid solution gadolinia-doped ceria from multiple virtual structures and isolated ion pairs [6,7]. Using the *ab initio* interionic potentials, we calculated the static properties of CeO_2, Gd_2O_3 and Ce_2O_3 as well as doped concentration and temperature dependence of lattice constants, diffusion coefficients, pair correlation functions and elastic constants, which are consistent with corresponding experimental measurements. In particular, because of the quantum-chemical technique, the potential can be used in solid solution due to the same function form and parameters of the identical ions [6,7]. The successful results motivate us to extend the methodology to other ionic solids. In this work, we mainly focus on the development of interionic potential for alkaline-earth oxides MgO and CaO, which are the most abundant components in the Earth's lower mantle and have been used typically for understanding bonding in ionic oxides [8].

To this end, extensive studies have been conducted to investigate the equation of state, B1–B2 phase transition, as well as temperature/pressure dependence properties of CaO and MgO [9–13]. For example, potential-induced breathing (PIB) model has been used to calculate most of the properties of alkaline-earth oxides [14,15]. The temperature and pressure dependence of equation of states was examined by using a breathing shell model [16]. In addition, by fitting the forces and stress tensor, an aspherical ion model (AIM) [17–19] was developed for various relevant minerals and melts of the Ca–Mg–Al–Si–O system. In most of the previous studies [15,16,19], the interionic potentials were fitted with an a priori function form, and the quality of the interionic potential was strongly dependent on the fitted properties. Different potential parameters may give divergent results [6]. Such outcomes may be due to the limitation of the empirical potential framework. On the other hand, some *ab initio* potentials for ionic solids have been developed based on the Chen–Mobius inversion [1–3]. This procedure is independent of experimental data; however, some drawbacks still exist. The interaction between cations and anions will cause uncertainty and different parameters of the potential on the same species of ions [2,6]. Therefore, the lattice inversion method is limited to the solid solution with identical ions.

In this paper, we propose a novel method to derive the interionic potential for CaO and MgO by accounting for the lattice inversion, quantum-chemical calculation and empirical three-body fitting. For simplicity, all the ions are assumed to be formally charged, i.e. Ca^{2+}, Mg^{2+} and O^{2-}. Such an assumption is to eliminate the influence of the difference in charges on uniform ions during the charge determination [6,7]. First of all, the relevant cubic structures of different phases are constructed. Then, we compute the pseudo-potential total energies by *ab initio* calculations. After that, the short-range interactions between cations and anions are directly extracted from the total energy difference by the lattice inversion

*Corresponding author. Email: Sunyi@hit.edu.cn

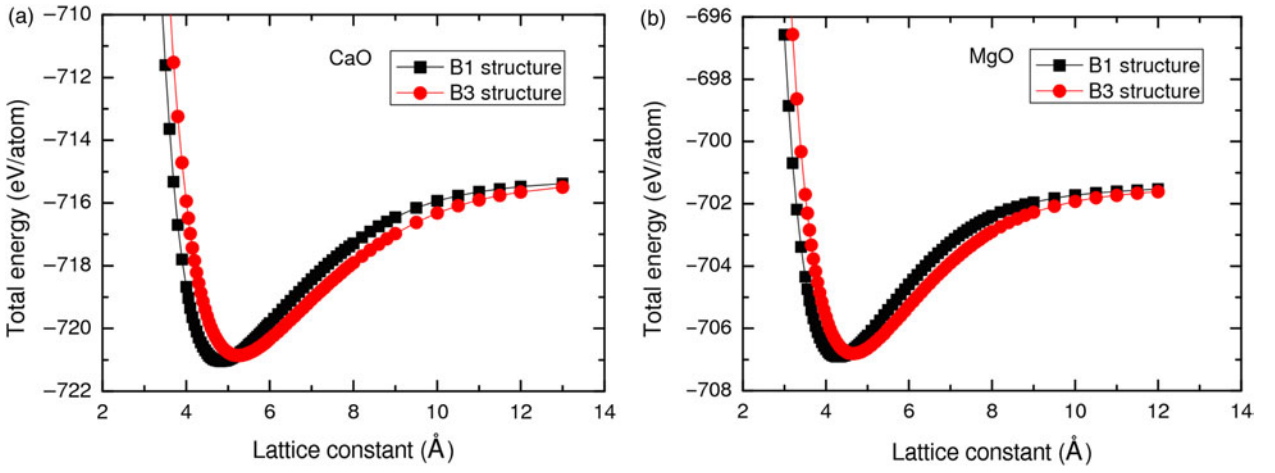

Figure 1. Total energies of CaO and MgO versus lattice constants.

approach. Meanwhile, the function form and parameters of the potential on the same species of ions are determined by fitting the deviation between the quantum-chemical calculations and Coulomb energy. Finally, the empirical three-body interactions are introduced to improve the mechanical properties by patching the mismatch between the pairwise potential and experimental measurements.

The paper is organised as follows: in Section 2, the development of interionic potential of AO (A = Ca, Mg) is presented. In Section 3, several molecular dynamics (MD) simulations, such as lattice constants, elastic constants and phase transformation, are carried out to validate the derived interionic potentials.

2. Development of interionic potential of AO (A = Ca, Mg)

2.1 Lattice inversion for interionic potentials between cations and anions

Consider a system of N ions and the pairwise energy is

$$E^{\text{pair}} = E^{\text{Coul}} + E^{\text{SP}} = E^{\text{Coul}} + E^{\text{SP}}_{++} + E^{\text{SP}}_{--} + E^{\text{SP}}_{+-}, \quad (1)$$

where E^{Coul} is the Coulomb energy, which could be evaluated by the Ewald summation technique or Wolf method [20]. E^{SP}represents the short-range interactions between different elements, which means that we cannot calculate each term on the right hand side of Equation (1) by only one individual structure. Some virtual structures are required to introduce more configurations and interionic spacing. It is noteworthy that these virtual structures must have identical sublattices constructed by cations and anions, which is aimed at eliminating the interactions between the identical ions.

At room temperature, pure AO is the rock salt structure. Hence, the prototypical structure of AO is chosen to be of B1-type. Another related structure should be given to obtain the short-range interaction between A^{2+} and O^{2-}. These two structures have the same ion arrangement, i.e. the sublattices of cations and anions are both face centre cubic. Here, the zinc blende structure (B3-type) is taken as the secondary structure [3].

Figure 1 shows the total energies of the above-mentioned structures versus lattice constant a, where $a = 4.0–13.0$ Å. They are calculated by the CASTEP program [21], using ultrasoft pseudo-potentials together with Perdew–Burke–Ernzerhof generalised gradient approximations exchange, i.e. correlation function. The k-mesh points over the Brillouin zone are generated with parameters $11 \times 11 \times 11$ for the biggest reciprocal space and $3 \times 3 \times 3$ for the smallest one by the Monkhorst–Pack mesh. A plane-wave basis set with 380 eV/atom cutoff is applied. The energy tolerance for self-consistent field convergence is 5.0×10^{-7} eV/atom for all calculations.

Based on our previous work [6], the inversion coefficients of the B1 and B3 structures can be expressed as follows:

$$E^{\text{SP}}_{\text{B1}(+-)} = E^{\text{tot}}_{\text{B1}} - E^{\text{Coul}}_{\text{B1}} - E^{\text{iso}}_{\text{B1}} = \frac{1}{2}\sum_{i,j,k}\Phi^{\text{SP}}_{+-}\left[\sqrt{(i+j-1.0)^2+(j+k-1.0)^2+(k+i-1.0)^2}\,\frac{a}{2}\right], \quad (2)$$

$$E^{\text{SP}}_{\text{B3}(+-)} = E^{\text{tot}}_{\text{B3}} - E^{\text{Coul}}_{\text{B3}} - E^{\text{iso}}_{\text{B3}} = \frac{1}{2}\sum_{i,j,k}\Phi^{\text{SP}}_{+-}\left[\sqrt{(i+j-0.5)^2+(j+k-0.5)^2+(k+i-0.5)^2}\,\frac{a}{2}\right], \quad (3)$$

where E^{tot} denotes the total energies obtained by the CASTEP program and E^{iso} denotes the energy of isolated ions, which is independent on interionic separation [1–3,6].

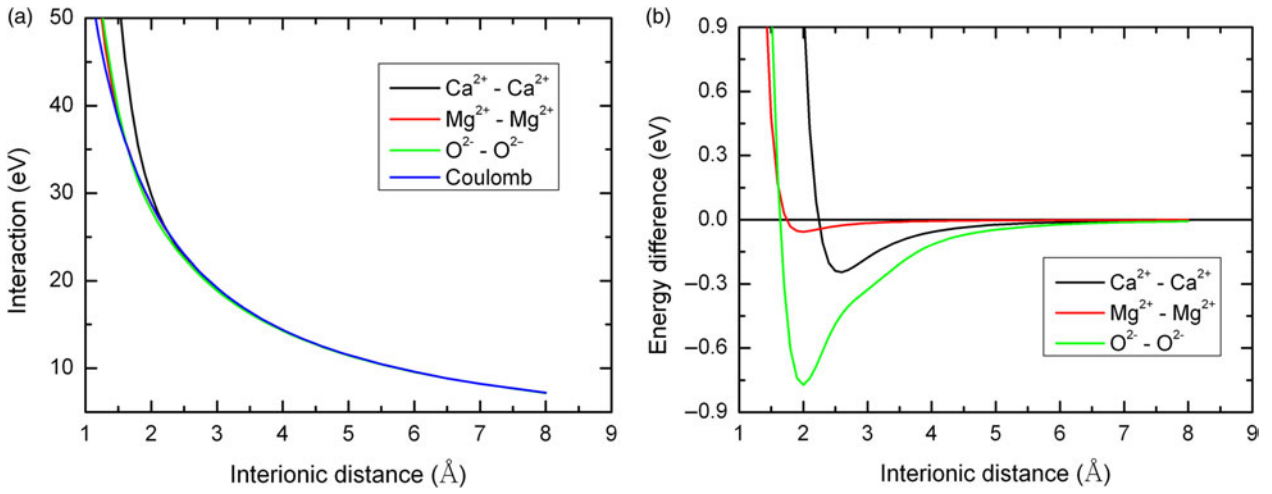

Figure 2. (Colour online) Comparison of Ca^{2+} ions, Mg^{2+} ions and O^{2-} ions between Gaussian03 calculation and Coulomb interaction.

By using Equations (2) and (3), we evaluated the short-range pairwise potential $\Phi^{SP}_{+-}(r)$ between cations and anions directly by the Chen–Mobius lattice inversion [1]. Such technique can also be applied for the derivation of the potentials between the same species of ions. However, it is not practical in the case of atomic motion of solid solution due to their distinct forms and parameters [2,6]. Hence, the quantum-chemical method is used to derive the potential between two identical ions in the following section.

2.2 *Quantum-chemical calculation for potential between uniform ions*

The GAUSSIAN03 [22] software is used for the quantum-chemical calculation. A correlation method, QCISD (T, Full)/6-311G, is applied for the model chemistry and basis set. In order to obtain the short-range interaction between uniform ions, the total charge and spin multiplicity S (number of lone pair electrons + 1) for each ion configuration should be specified. Because all ions are assumed to be formally charged, the outer electron shell of ion is fully occupied, i.e. the spin multiplicity S is always 1. The following two consecutive steps were conducted to derive the interionic potential: (1) determination of the isolated ion energy and (2) comparison with pair ions energy and formal charged Coulomb energy.

Figure 2 shows the energies corresponding to the interionic separation r_{ij} of Ca^{2+}, Mg^{2+} and O^{2-} ions. Clearly, the computed quantum-chemical results are very close to the Coulomb energies, which imply that the total charge of the system is distributed uniformly on each atom. In addition, the difference between Coulomb and *ab initio* calculations can be considered as the short-range interionic potential of the same species of ions. Apparently, the potential is negligible once the separation is larger than 6 Å, indicating a pure Coulombic interaction between two identical ions in a gaseous phase. Note that the potentials could be applied in all structures, because the *ab initio* calculations are independent of a specific lattice structure. The forms and parameters of the potential function, which are only dependent on the discrete energy values, show much better portability, especially in solid solution system [6].

2.3 *Pairwise potential function forms and parameters*

The short-range pair potential curves can be extracted from lattice inversion and quantum-chemical calculations. The suitable potential function forms are selected to fit the potential curves. In this study, the following short-range potential function forms are utilised:

$$\begin{aligned}\Phi_{+-}(r) &= \Phi^{SP}_{+-}(r) + \Phi^{Coul}_{+-}(r) \\ &= a_{+-}\exp\left[b_{+-}\left(1-\frac{r}{c_{+-}}\right)\right] + \frac{q_+q_-}{4\pi\varepsilon_0 r},\end{aligned} \tag{4}$$

$$\begin{aligned}\Phi_{--}(r) &= \Phi^{SP}_{--}(r) + \Phi^{Coul}_{--}(r) \\ &= a_{--}\left\{\left(\exp\left[\frac{b_{--}}{2}\left(1-\frac{r}{c_{--}}\right)\right]-1\right)^2-1\right\} + \frac{q_-^2}{4\pi\varepsilon_0 r},\end{aligned} \tag{5}$$

$$\begin{aligned}\Phi_{++}(r) &= \Phi^{SP}_{++}(r) + \Phi^{Coul}_{++}(r) \\ &= a_{++}\left\{\left(\exp\left[\frac{b_{++}}{2}\left(1-\frac{r}{c_{++}}\right)\right]-1\right)^2-1\right\} + \frac{q_+^2}{4\pi\varepsilon_0 r},\end{aligned} \tag{6}$$

where $\Phi^{SP}_{+-}(r)$ is the exponent repulsive. $\Phi^{SP}_{--}(r)$ and $\Phi^{SP}_{++}(r)$ are Morse functions. Parameters a, b and c for different cases are tabulated in Table 1.

Table 1. Parameters of the short-range interaction.

Species	a (eV)	b	c (Å)
Ca^{2+}–O^{2-}	0.20	8.17326	3.12508
Mg^{2+}–O^{2-}	0.20	7.9910	2.86464
Ca^{2+}–Ca^{2+}	0.24760	10.13505	2.58565
Mg^{2+}–Mg^{2+}	0.05657	10.56375	1.98963
O^{2}–O^{2-}	0.77109	7.85216	1.99458

2.4 *Three-body potential model*

The static properties of equilibrium of AO at zero temperature and pressure can be computed by pairwise potential. It is found that (shown in Table 3) the potentials can describe the structures of CaO and MgO approximately but with unphysical Cauchy relation ($C_{12} = C_{44}$). Thus, some three-body interactions are needed to eliminate the drawbacks arising from the pairwise potentials. In this study, it is anticipated to derive an effective three-body potential function by fitting the elastic constants. For simplicity, the short-range three-body potential Φ^{ST} is assumed to be neglected beyond the nearest neighbour (NN) distance. For a three-body potential, $\Phi^{ST}(r_{ij}, r_{ik}, \theta_{ijk})$, its corresponding elastic constants can be obtained by

$$C_{11}^{ST} = \left(\frac{\partial^2 \Phi^{ST}(a)}{\partial \varepsilon_1^2}\right)_{a=a_0}, \quad C_{12}^{ST} = \left(\frac{\partial^2 \Phi^{ST}(a)}{\partial \varepsilon_1 \, \partial \varepsilon_2}\right)_{a=a_0},$$
$$C_{44}^{ST} = \left(\frac{\partial^2 \Phi^{ST}(a)}{\partial \varepsilon_4^2}\right)_{a=a_0}, \tag{7}$$

where ε_i is the strain tensor. The three-body potential is assumed as

$$\Phi^{ST}(r_{ij}, r_{ik}, \theta_{ijk}) = f(r_{ij}, r_{ik}) g(\theta_{ijk}) = f(r_{ij}, r_{ik}) g(\cos\theta_{ijk}), \tag{8}$$

where

$$\cos\theta = \frac{\vec{r}_{ij} \cdot \vec{r}_{ik}}{r_{ij} r_{ik}} = \frac{A(\varepsilon)}{r_{ij} r_{ik}} \tag{9}$$

and

$$\begin{aligned}\vec{r}_{ij} \cdot \vec{r}_{ik} = A(\varepsilon) = \vec{r}_{ij0} \cdot \vec{r}_{ik0} + a_0^2 \{ & 2\varepsilon_1 r_{ijx} r_{ikx} + 2\varepsilon_2 r_{ijy} r_{iky} \\ & + 2\varepsilon_3 r_{ijz} r_{ikz} \quad + \varepsilon_4 (r_{ijy} r_{ikz} + r_{ijz} r_{iky}) \\ & + \varepsilon_5 (r_{ijx} r_{ikz} + r_{ijz} r_{ikx}) + \varepsilon_6 (r_{ijy} r_{ikx} + r_{ijx} r_{iky}) \}.\end{aligned} \tag{10}$$

Here, r_0 and a_0 are the nearest distance and lattice constant of equilibrium state, respectively. r_{ix}, r_{iy} and r_{iz} are the ith atomic coordinates in x, y and z directions, respectively. According to Equation (7), the elastic constants of three-body potential C_{11}^{ST}, C_{12}^{ST} and C_{44}^{ST} can be derived as

$$\begin{aligned} C_{11}^{ST} = \frac{\partial^2 \Phi^{ST}}{\partial \varepsilon_1^2} = a_0^4 \times & \left(\left(\left(\frac{\partial^2 f}{\partial r_{ij}^2} \right) \left(\frac{r_{ijx}^4}{r_{ij}^2} \right) \right. \right. \\ & + 2 \left(\frac{\partial^2 f}{\partial r_{ij} \, \partial r_{ik}} \right) \left(\frac{r_{ijx}^2 r_{ikx}^2}{r_{ij} r_{ik}} \right) + \left(\frac{\partial^2 f}{\partial r_{ik}^2} \right) \left(\frac{r_{ikx}^4}{r_{ik}^2} \right) \Big) g \\ & + \left(\left(\frac{\partial f}{\partial r_{ij}} \right) \left(- \frac{r_{ijx}^4}{r_{ij}^3} \right) + \left(\frac{\partial f}{\partial r_{ik}} \right) \left(- \frac{r_{ikx}^4}{r_{ik}^3} \right) \right) g \\ & + 2 \left(\left(\frac{\partial f}{\partial r_{ij}} \right) \left(\frac{r_{ijx}^2}{r_{ij}} \right) + \left(\frac{\partial f}{\partial r_{ik}} \right) \left(\frac{r_{ikx}^2}{r_{ik}} \right) \right) \left(\frac{2 r_{ijx} r_{ikx}}{r_{ij} r_{ik}} \right. \\ & \left. - \left(\frac{r_{ijx}^2}{r_{ij}^2} + \frac{r_{ikx}^2}{r_{ik}^2} \right) \cos\theta \right) \frac{\partial g}{\partial \cos\theta} \\ & + f \left(\left(3 \frac{r_{ijx}^4}{r_{ij}^4} + 2 \frac{r_{ijx}^2 r_{ikx}^2}{r_{ij}^2 r_{ik}^2} + 3 \frac{r_{ikx}^4}{r_{ik}^4} \right) \cos\theta \right. \\ & \left. - \left(\frac{r_{ijx}^2}{r_{ij}^2} + \frac{r_{ikx}^2}{r_{ik}^2} \right) \frac{4 r_{ijx} r_{ikx}}{r_{ij} r_{ik}} \right) \frac{\partial g}{\partial \cos\theta} \\ & + f \left(\frac{2 r_{ijx} r_{ikx}}{r_{ij} r_{ik}} - \left(\frac{r_{ijx}^2}{r_{ij}^2} + \frac{r_{ikx}^2}{r_{ik}^2} \right) \cos\theta \right)^2 \frac{\partial^2 g}{\partial \cos^2\theta} \Big), \end{aligned} \tag{11}$$

$$\begin{aligned} C_{12}^{ST} = \frac{\partial^2 \Phi^{ST}}{\partial \varepsilon_1 \, \partial \varepsilon_2} = a_0^4 \times & \left(\left(\left(\frac{\partial^2 f}{\partial r_{ij}^2} \right) \left(\frac{r_{ijx}^2 r_{ijy}^2}{r_{ij}^2} \right) + \left(\frac{\partial^2 f}{\partial r_{ik}^2} \right) \left(\frac{r_{ikx}^2 r_{iky}^2}{r_{ik}^2} \right) \right) g \right. \\ & + \left(\frac{\partial^2 f}{\partial r_{ij} \, \partial r_{ik}} \right) \left(\frac{r_{ijx}^2 r_{iky}^2 + r_{ijy}^2 r_{ikx}^2}{r_{ij} r_{ik}} \right) g \\ & + \left(\left(\frac{\partial f}{\partial r_{ij}} \right) \left(- \frac{r_{ijx}^2 r_{ijy}^2}{r_{ij}^3} \right) + \left(\frac{\partial f}{\partial r_{ik}} \right) \left(- \frac{r_{ikx}^2 r_{iky}^2}{r_{ik}^3} \right) \right) g \\ & + \left(\left(\frac{\partial f}{\partial r_{ij}} \right) \left(\frac{r_{ijx}^2}{r_{ij}} \right) + \left(\frac{\partial f}{\partial r_{ik}} \right) \left(\frac{r_{ikx}^2}{r_{ik}} \right) \right) \left(\frac{2 r_{ijy} r_{iky}}{r_{ij} r_{ik}} \right. \\ & \left. - \left(\frac{r_{ijy}^2}{r_{ij}^2} + \frac{r_{iky}^2}{r_{ik}^2} \right) \cos\theta \right) \frac{\partial g}{\partial \cos\theta} \\ & + \left(\left(\frac{\partial f}{\partial r_{ij}} \right) \left(\frac{r_{ijy}^2}{r_{ij}} \right) + \left(\frac{\partial f}{\partial r_{ik}} \right) \left(\frac{r_{iky}^2}{r_{ik}} \right) \right) \left(\frac{2 r_{ijx} r_{ikx}}{r_{ij} r_{ik}} \right. \\ & \left. - \left(\frac{r_{ijx}^2}{r_{ij}^2} + \frac{r_{ikx}^2}{r_{ik}^2} \right) \cos\theta \right) \frac{\partial g}{\partial \cos\theta} \\ & + f \left(\left(3 \frac{r_{ijx}^2 r_{ijy}^2}{r_{ij}^4} + \frac{r_{ijx}^2 r_{iky}^2 + r_{ijy}^2 r_{ikx}^2}{r_{ij}^2 r_{ik}^2} + 3 \frac{r_{ikx}^2 r_{iky}^2}{r_{ik}^4} \right) \cos\theta \right) \frac{\partial g}{\partial \cos\theta} \\ & + f \left(- \left(\frac{r_{ijy}^2}{r_{ij}^2} + \frac{r_{iky}^2}{r_{ik}^2} \right) \frac{2 r_{ijx} r_{ikx}}{r_{ij} r_{ik}} - \left(\frac{r_{ijx}^2}{r_{ij}^2} + \frac{r_{ikx}^2}{r_{ik}^2} \right) \frac{2 r_{ijy} r_{iky}}{r_{ij} r_{ik}} \right) \frac{\partial g}{\partial \cos\theta} \\ & + f \left(\frac{2 r_{ijx} r_{ikx}}{r_{ij} r_{ik}} - \left(\frac{r_{ijx}^2}{r_{ij}^2} + \frac{r_{ikx}^2}{r_{ik}^2} \right) \cos\theta \right) \left(\frac{2 r_{ijy} r_{iky}}{r_{ij} r_{ik}} \right. \\ & \left. \left. - \left(\frac{r_{ijy}^2}{r_{ij}^2} + \frac{r_{iky}^2}{r_{ik}^2} \right) \cos\theta \right) \frac{\partial^2 g}{\partial \cos^2\theta} \right), \end{aligned} \tag{12}$$

$$
\begin{aligned}
C_{44}^{\mathrm{ST}} = \frac{\partial^2 \Phi^{\mathrm{ST}}}{\partial \varepsilon_4^2} = a_0^4 \times \Bigg(& \left(\left(\frac{\partial^2 f}{\partial r_{ij}^2} \right) \left(\frac{r_{ijy}^2 r_{ijz}^2}{r_{ij}^2} \right) \right. \\
& \left. + 2 \left(\frac{\partial^2 f}{\partial r_{ij} \partial r_{ik}} \right) \left(\frac{r_{ijy} r_{ijz} r_{iky} r_{ikz}}{r_{ij} r_{ik}} \right) + \left(\frac{\partial^2 f}{\partial r_{ik}^2} \right) \left(\frac{r_{iky}^2 r_{ikz}^2}{r_{ik}^2} \right) \right) g \\
& + \left(\left(\frac{\partial f}{\partial r_{ij}} \right) \left(- \frac{r_{ijy}^2 r_{ijz}^2}{r_{ij}^3} \right) + \left(\frac{\partial f}{\partial r_{ik}} \right) \left(- \frac{r_{iky}^2 r_{ikz}^2}{r_{ik}^3} \right) \right) g \\
& + 2 \left(\left(\frac{\partial f}{\partial r_{ij}} \right) \left(\frac{r_{ijy} r_{ijz}}{r_{ij}} \right) + \left(\frac{\partial f}{\partial r_{ik}} \right) \left(\frac{r_{iky} r_{ikz}}{r_{ik}} \right) \right) \\
& \times \left(\left(\frac{r_{ijy} r_{ikz} + r_{ijz} r_{iky}}{r_{ij} r_{ik}} \right) - \left(\frac{r_{ijy} r_{ijz}}{r_{ij}^2} + \frac{r_{iky} r_{ikz}}{r_{ik}^2} \right) \cos\theta \right) \frac{\partial g}{\partial \cos\theta} \\
& + f \left(\left(3 \frac{r_{ijy}^2 r_{ijz}^2}{r_{ij}^4} + 2 \frac{r_{ijy} r_{ijz} r_{iky} r_{ikz}}{r_{ij}^2 r_{ik}^2} + 3 \frac{r_{iky}^2 r_{ikz}^2}{r_{ik}^4} \right) \cos\theta \right) \frac{\partial g}{\partial \cos\theta} \\
& + f \left(-2 \left(\frac{r_{ijy} r_{ijz}}{r_{ij}^2} + \frac{r_{iky} r_{ikz}}{r_{ik}^2} \right) \left(\frac{r_{ijy} r_{ikz} + r_{ijz} r_{iky}}{r_{ij} r_{ik}} \right) \right) \frac{\partial g}{\partial \cos\theta} \\
& + f \left(\left(\frac{r_{ijy} r_{ikz} + r_{ijz} r_{iky}}{r_{ij} r_{ik}} \right) - \left(\frac{r_{ijy} r_{ijz}}{r_{ij}^2} + \frac{r_{iky} r_{ikz}}{r_{ik}^2} \right) \cos\theta \right)^2 \frac{\partial^2 g}{\partial \cos^2 \theta} \Bigg).
\end{aligned}
\tag{13}
$$

The three-body potential can be fitted directly with Equations (11)–(13) once we know the difference of elastic constants between pair potential and experimental data. Here, the three-body function Φ^{ST} is assumed as either $\Phi^{\mathrm{ST}}(r_{ij}, r_{ik}, \theta_{ijk}) = [f(r_{ij}) + f(r_{ik})] g(\theta_{ijk})$ (ADD) or $\Phi^{\mathrm{ST}}(r_{ij}, r_{ik}, \theta_{ijk}) = f(r_{ij}) f(r_{ik}) g(\theta_{ijk})$ (MUL). Because of the rock salt structure of AO, we have $\Phi^{\mathrm{ST}}_{\mathrm{A-O-A}}(r_{ij}, r_{ik}, \theta_{ijk}) = \Phi^{\mathrm{ST}}_{\mathrm{O-A-O}}(r_{ij}, r_{ik}, \theta_{ijk})$. The elastic constants of Φ^{ST} are: (1) only MUL can modify the C_{12} with $g(\theta) = 1$, (2) MUL and ADD are used to adjust the elastic constant C_{11} in the case of $g(\theta) = \cos\theta$ and (3) MUL and ADD can modify the C_{44} with $g(\theta) = \cos^2\theta + \cos^3\theta$. Clearly, the components in three-body interactions are fully decoupled. Based on the analysis above, the three-body interaction can be rewritten as

$$
\begin{aligned}
\Phi^{\mathrm{ST}} = & \lambda_1 \exp\left[\gamma_1 \left(1 - \frac{r_{ij}}{\eta} \right) \right] \exp\left[\gamma_1 \left(1 - \frac{r_{ik}}{\eta} \right) \right] (1 + \cos\theta) \\
& + \lambda_2 \left\{ \exp\left[\gamma_2 \left(1 - \frac{r_{ij}}{\eta} \right) \right] + \exp\left[\gamma_2 \left(1 - \frac{r_{ik}}{\eta} \right) \right] \right\} \\
& + \lambda_3 \left\{ \exp\left[\gamma_3 \left(1 - \frac{r_{ij}}{\eta} \right) \right] + \exp\left[\gamma_3 \left(1 - \frac{r_{ik}}{\eta} \right) \right] \right\} \\
& + \lambda_4 \left\{ \exp\left[\gamma_4 \left(1 - \frac{r_{ij}}{\eta} \right) \right] + \exp\left[\gamma_4 \left(1 - \frac{r_{ik}}{\eta} \right) \right] \right\} (\cos^2\theta + \cos^3\theta).
\end{aligned}
\tag{14}
$$

Here, the first term on the right hand side is used to modify the C_{12} of AO, whereas the second and third terms are to correct C_{11} and lattice constants. The elastic constant C_{44} is adjusted by the last term in Equation (14). All the parameters in this equation are listed in Table 2.

3. Application of interionic potentials

3.1 *Static properties*

By using the developed interionic potentials, we computed the static properties of the equilibrium of B1-AO structures at zero temperature and pressure, such as lattice constants, lattice energy and elastic properties, and are illustrated in Table 3. The results obtained from the CASTEP calculation and other empirical functions are also presented for comparison. Clearly, a good agreement is achieved.

For further validity of our developed interionic potentials, the physical properties of the B2-AO structure are also calculated, as displayed in Table 4. The lattice constant of CaO is very close to the experimental data at the pressure of 60 GPa, which reveals that our potential can predict the properties of other phases accurately. Thus, it is evident that our interionic potential is robust.

3.2 *AO at 0 K under high pressure*

The pressure dependence of physical properties is also investigated to verify the developed interionic potential. The results are depicted in Figures 3–5. Owing to lack of experiment results, the *ab initio* calculations are carried out for comparison. In the pressure range from 0 to 200 GPa, the lattice constants (Figure 3) and elastic constants (Figure 4) of the MD and *ab initio* calculations show the same trend with small discrepancy. The slightly large values by *ab initio* calculation may be attributed to the larger lattice constant obtained at zero temperature and pressure than that from experiments. Moreover, note that from 0 to 200 GPa, the lattice constant reduces gradually from 4.2 to 3.6 Å for MgO and from 4.8 to 4.0 Å for CaO (Figure 3). This reveals that our interionic potential could describe the evolution of materials behaviours in extended phase space.

Cauchy relation, i.e. $C_{12} = C_{44} + 2P$, is regarded as a measure of the contribution from the many-body interaction. Figure 5 shows the Cauchy violation as a

Table 2. Parameters of the short-range three-body potential for CaO and MgO.

	λ (eV)				γ				
	λ_1	λ_2	λ_3	λ_4	γ_1	γ_2	γ_3	γ_4	η(Å)
CaO	−2.2244	0.03855	2.7459	−5.439	2.1561	1.078	7.0684	5.4546	1.195
MgO	−2.6333	0.08512	1.0496	0.045	1.9096	0.9548	6.2062	0.9096	1.054

Table 3. Static properties of CaO and MgO in rock salt structure.

		Lattice constant (Å)	Bulk modulus (GPa)	Lattice energy (eV)	Elastic constants (GPa)		
					C_{11}	C_{12}	C_{44}
CaO	This work (only pair)	4.853	117.3	17.50	192.9	79.5	79.5
	This work (0 K)	4.792	116.5	17.39	233.7	57.9	79.3
	This work (300 K)	4.810	110.6		220.0	56.4	76.9
	Wang [3]	4.842	129.8	17.46	235.5	77.0	99.2
	AIM [19]	4.809	116.1		231.9	58.2	73.0
	PIB [14]	4.820	102.0	15.05	206.0	50.0	66.0
	Expt [9]	4.810	114.0	18.70	220.6	56.6	80.3
	CASTEP	4.837	103.3		198.1	55.9	75.2
MgO	This work (only pair)	4.312	173.7	19.54	252.5	134.3	134.3
	This work (0 K)	4.203	166.8	19.16	314.7	92.9	157.5
	This work (300 K)	4.216	158.5		295.3	90.1	154.9
	Zhang [23]	4.286	169.6	18.98	314.9	97.0	169.0
	Karki [11]	4.251	158		291	91	139
	Matsui [24]	4.212	161		294	94	157
	Expt [25,26]	4.216	162.2	20.05	295.9	95.4	153.9
	CASTEP	4.286	145.9		257.2	90.3	135.2

Table 4. Static properties of CaO and MgO in CsCl structure.

		Lattice constant (Å)	Lattice energy (eV)	Bulk modulus (GPa)
CaO	This work	2.883	16.83	135.2
	Wang [3]	2.955	16.45	154.0
	MPIB [15]	2.890	13.75	140.0
	CASTEP	2.937		105.8
CaO (60 GPa)	This work	2.644		
	Wang [3]	2.727		
	Expt [10]	2.642		
MgO	This work	2.567	17.99	174.3
	Baltache [27]	2.604		163
	CASTEP	2.681		135.8

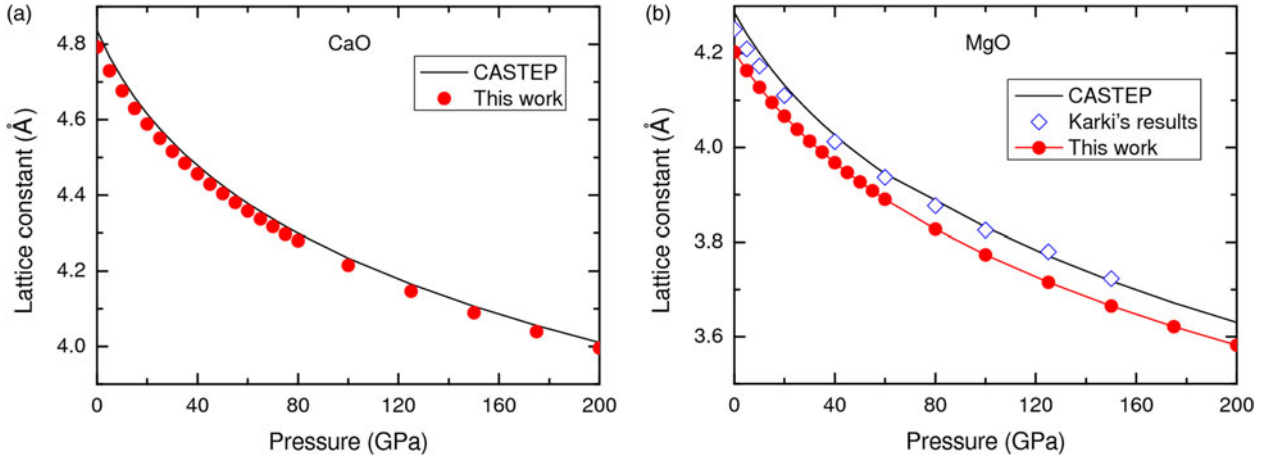

Figure 3. Comparison of lattice constants for CaO and MgO.

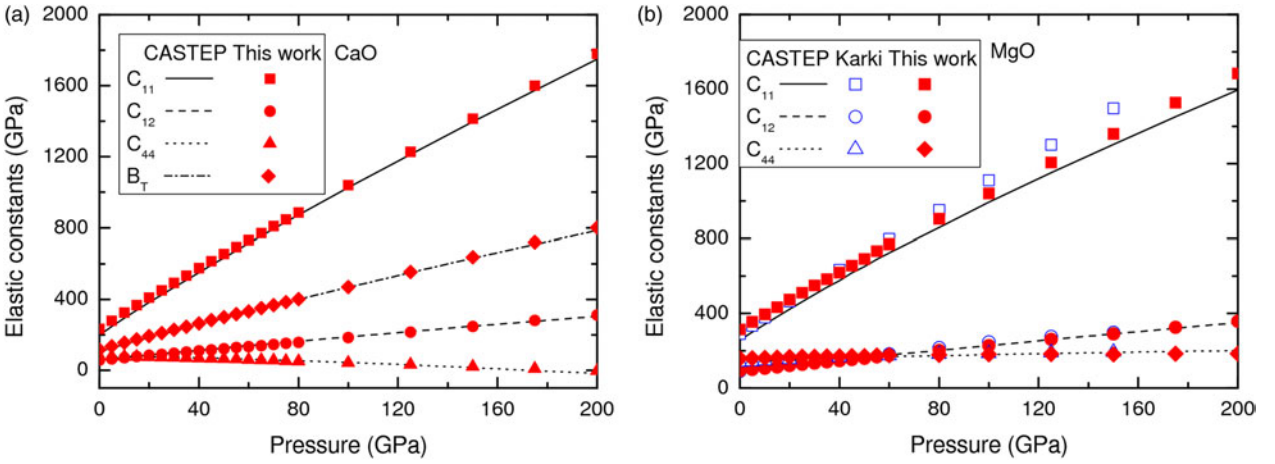

Figure 4. Comparison of elastic constants for CaO and MgO.

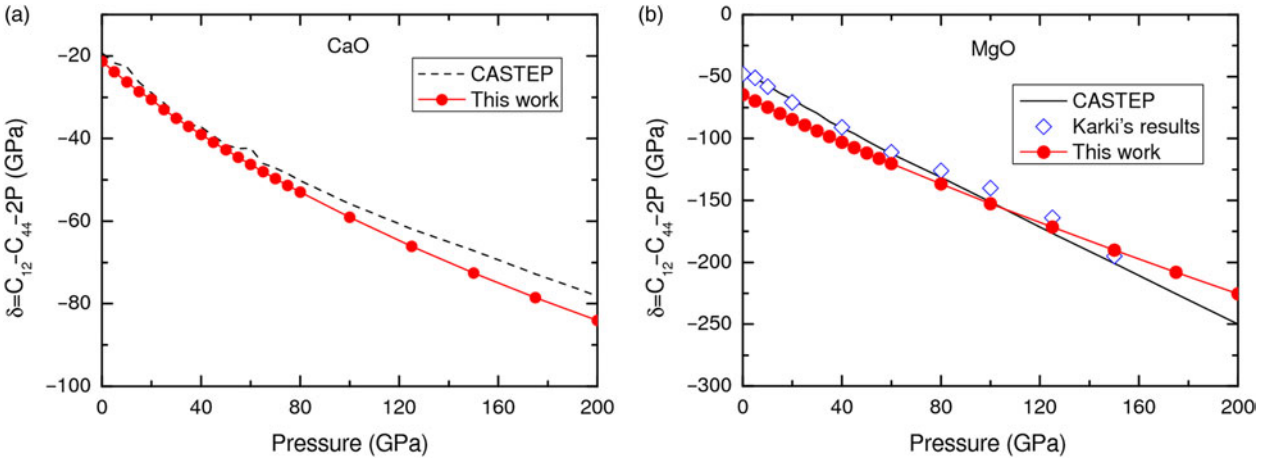

Figure 5. Comparison of Cauchy violation for CaO and MgO.

function of applied pressure. The deviation tends to be larger with the increment of pressure, which indicates that the many-body force becomes more profound at high pressure.

3.3 Phase transition

It is well known that AO is a rock salt crystalline and can be transformed into a CsCl-type structure under high pressure. Some first-principles calculations have been carried out to study such phase transition, for instance, 60–70 GPa for CaO [10,28,29] and 400–486 GPa for MgO [11,13,30].

Figure 6 shows the calculated energy per atom versus volume per atom for both B1 and B2 phases. Obviously, the B1 phase is stable at low-pressure regime, whereas the B2 structure is more favourable at high-pressure regime. To investigate the B1–B2 phase transition in AO, we calculated the enthalpy ($E + PV$) of both B1 and B2 structures as a function of pressure (0–200 GPa for CaO, and 0–800 GPa for MgO). The crossing points of the enthalpy curves shown in Figure 7 determine the critical pressures in which the phase transition from B1 to B2 occurs. They are 67.99 GPa for CaO and 400.4 GPa for MgO, which are very close to experimental results [10] and *ab initio* predictions [11,30].

We also calculated the variation of relative volume with pressure for B1 and B2 phases. For CaO, the volume of B1 phase is reduced by 27%, which is consistent with the *ab initio* calculations [31]. The volume reduction of MgO is approximately 50% over the pressure range 0–400 GPa. The volume change of MgO from B1 phase to B2 phase is 0.665 $Å^3$, which is smaller than that of Karki's values 0.458 $Å^3$. This may be due to the larger transition pressure predicted by *ab initio* [11].

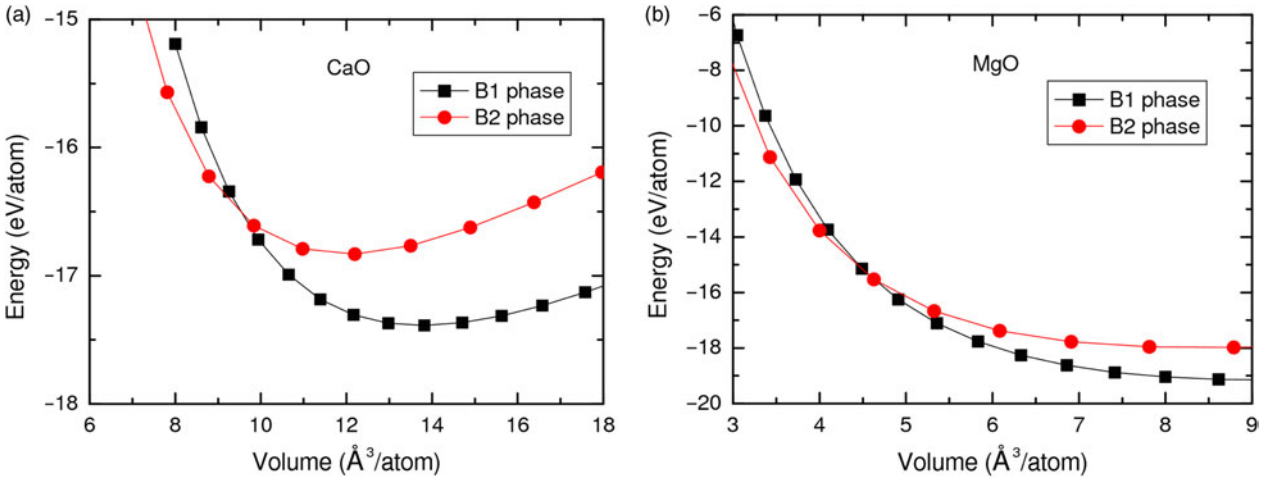

Figure 6. Total energy per atom versus volume per atom for B1 and B2 phases.

Figure 8 shows the calculated elastic constants of B1 and B2 phases as a function of applied pressure. It is seen that C_{11} is more sensitive to pressure than C_{12} and C_{44}. This is because C_{11} represents elasticity in length, whereas C_{12} and C_{44} are associated with the elasticity in shape. At the pressure of 70 GPa, the shear deformation of MgO is prone to occur along the (100) plane because $C_{11} > C_{12} > C_{44}$ [13]. A similar phenomenon for CaO takes place at a pressure of 15 GPa. In addition, both B1 and B2 phases are elastically stable, i.e. $C_{11} > 0$, $C_{11} > C_{12}$ and $C_{44} > 0$ [32]. This is also in agreement with other literature [13].

The elastic properties of isotropic polycrystalline material are unique because of two elastic stiffness coefficients, namely, the bulk (B) and the shear (G) modulus [11]. They can be computed as follows:

$$B = \frac{C_{11} + 2C_{12}}{3} \quad \text{and} \quad G = \frac{1}{2}(G_U + G_L), \tag{15}$$

$$G_U = C_{44} + 2\left[\frac{5}{C_S - C_{44}} + \frac{18(B + 2C_{44})}{5C_{44}(3B + 4C_{44})}\right], \tag{16}$$

$$G_L = C_S + 3\left[\frac{5}{C_{44} - C_S} + \frac{12(B + 2C_S)}{5C_S(3B + 4C_S)}\right], \tag{17}$$

where $C_S = (C_{11} - C_{12})/2$. The dependence of the modulus for AO under pressure is explored and the results are shown in Figure 9. A linear relationship between the modulus and pressure is detected. The bulk and shear modulus of the B2 phase are relatively larger than those of

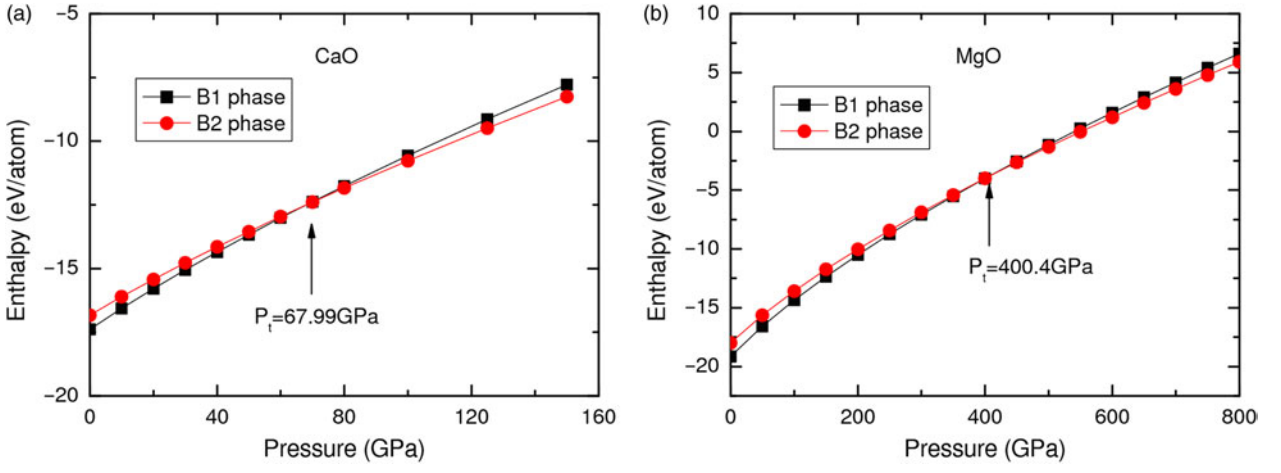

Figure 7. Enthalpy per atom versus volume per atom for B1 and B2 phases.

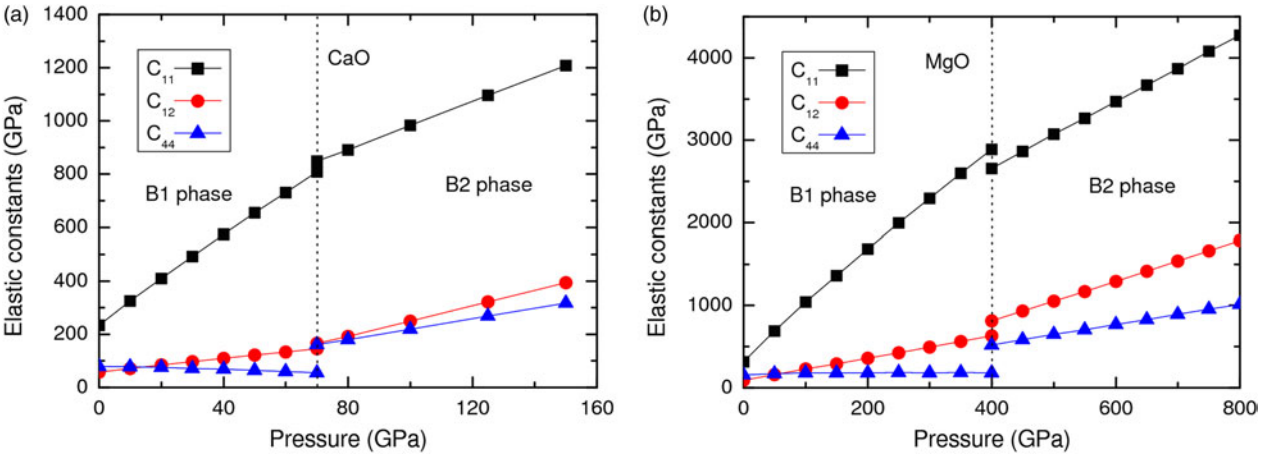

Figure 8. Dependence of elastic constants on hydrostatic pressure of CaO and MgO.

the B1 phase, which may be caused by larger C_{12} and C_{44} of B2.

The effect of pressure on the propagation of elastic waves in materials provides insights for understanding interatomic interactions. The elastic constants completely specify the mechanical properties and acoustic velocities of a crystal structure. The dependence of wave velocities upon hydrostatic pressure has been reported [11,13]. In fact, the longitudinal and shear wave velocities V_p and V_s can be extracted by

$$V_p = \sqrt{\frac{B + 4G/3}{\rho}} \quad \text{and} \quad V_s = \sqrt{\frac{G}{\rho}}, \tag{18}$$

where ρ is the density of the material.

Figure 10 shows the calculated acoustic velocities of AO as a function of pressure reflecting a typical linear relationship. This is reasonable because both the long wavelength longitudinal and shear acoustic modes stiffen under pressure. Furthermore, the longitudinal wave is faster than the shear wave in both B1 and B2 phases.

Finally, the anisotropy factor which is the ratio of C_{44} and $(C_{11} - C_{12})/2$ is determined for both B1 and B2 phases, as shown in Figure 11. The B1 phase exhibits low elastic anisotropy at zero pressure, and the degree of anisotropy increases with pressure. At low pressure, the anisotropy factor decreases dramatically with pressure, which is consistent with previous studies [12,33].

3.4 *AO at high temperature*

The MD simulations at finite temperatures are conducted to validate the robustness of developed interionic potential. The model used in our MD simulation includes 1000 ions ($5 \times 5 \times 5$ AO supercell). The NPT ensemble (fixed atom number, pressure and temperature) is adopted, implemented by Nose–Poincare thermostat [34], metric-tensor pressostat [35] and generalised leap-frog algorithm

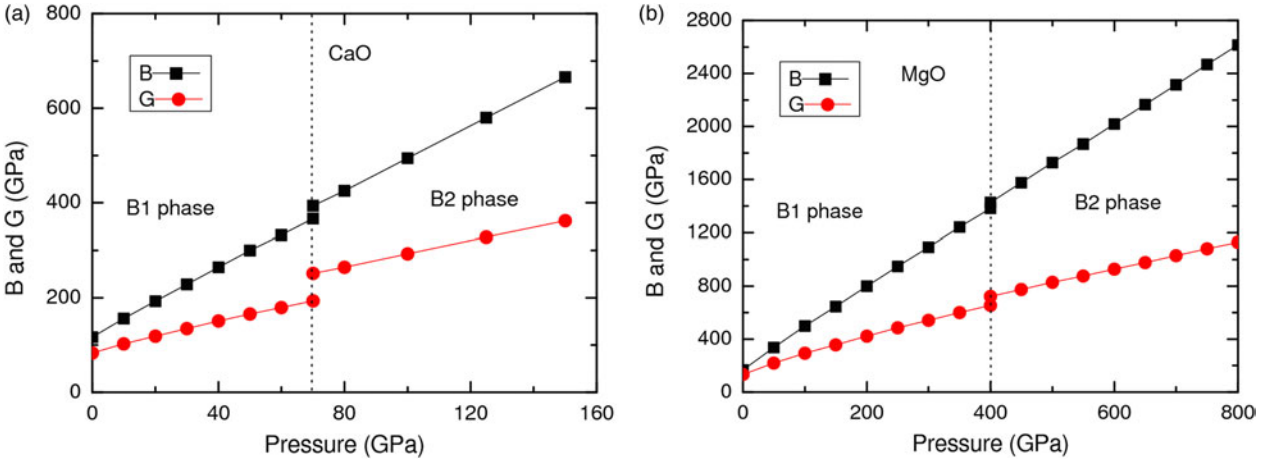

Figure 9. Bulk and the shear modulus as a function of pressure of CaO and MgO.

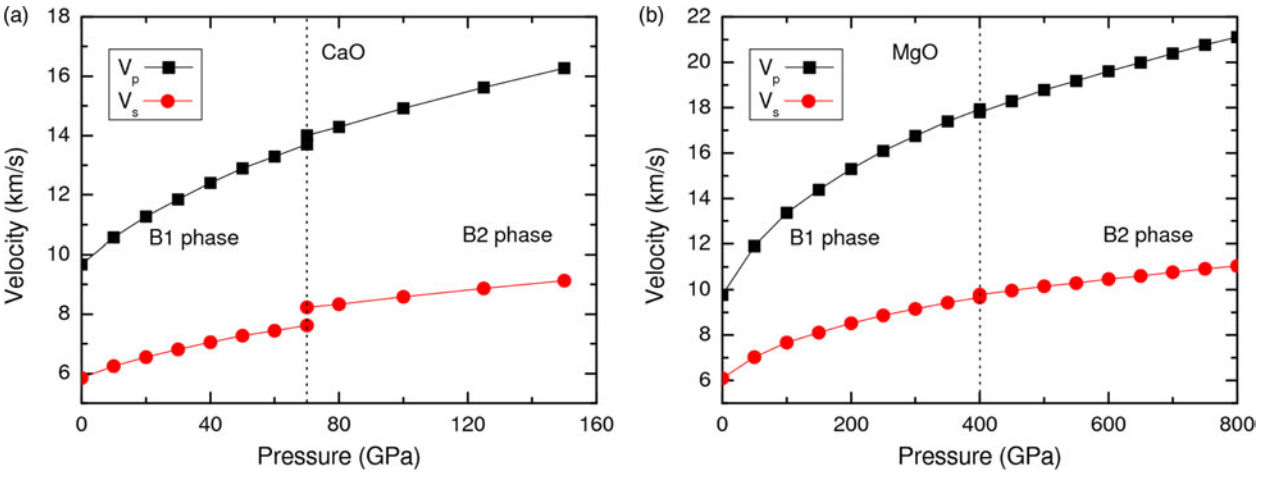

Figure 10. V_p and V_s velocities as a function of pressure of CaO and MgO.

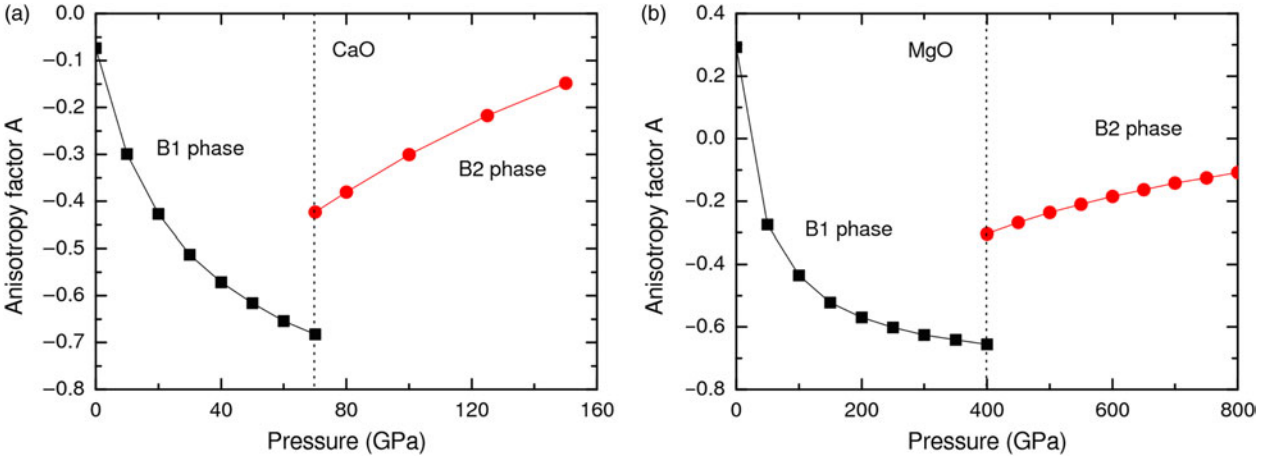

Figure 11. Anisotropy factor as a function of the pressure of CaO and MgO.

[36] for time integration. Wolf algorithm [20] is used to estimate the Coulomb interaction, and combination neighbour list algorithm [37] is adopted to increase the computational efficiency. The cutoff distance is set as 10.0 Å. The temperature for the simulation varies from 300 to 3000 K with an iteration of 100 K. The supercell model is equilibrated for 1×10^6 steps, and an additional 2×10^6 steps are used for data collection.

Figure 12 shows the volume expansion with the increment of temperature. The volume V_0 at 300 K and 0 Pa is calculated as the benchmark. In the intermediate temperature range (300–1200 K for CaO and 300–1800 K for MgO), our results match perfectly with Anderson's measurement [38]. At a higher temperature regime, our calculations are close to Fiquet's values [39].

Then, the elastic constants are evaluated by the stress and strain fluctuation formula [40] as shown in Figure 13. For better comparison, the experimental data are transformed by Equation (19) which show good agreement with our results

$$C_{11}^{S} - C_{11}^{T} = C_{12}^{S} - C_{12}^{T} = B_S - B_T \text{ and } C_{44}^{S} - C_{44}^{T} = 0. \quad (19)$$

4. Concluding remarks

In this paper, a novel method has been developed to derive the interionic potential for CaO and MgO by combining the benefits of Chen–Mobius lattice inversion, quantum-chemical calculation and empirical three-body interaction. This approach is anticipated to provide a bridging between *ab initio* potential and empirical functions. The *ab initio* calculations are used to obtain the short-range pairwise potentials, whereas the three-body interactions are

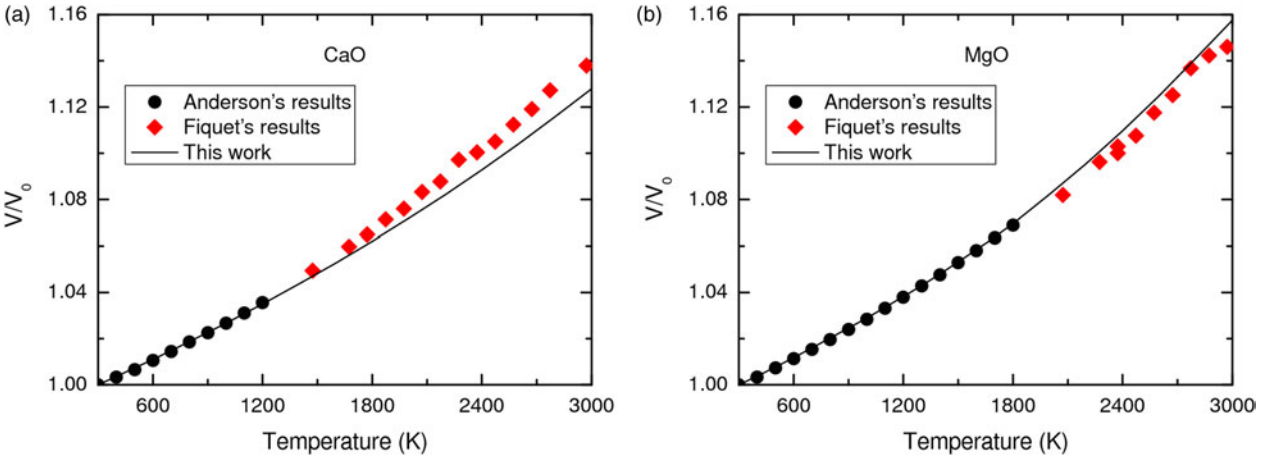

Figure 12. Temperature dependence of volume for CaO and MgO.

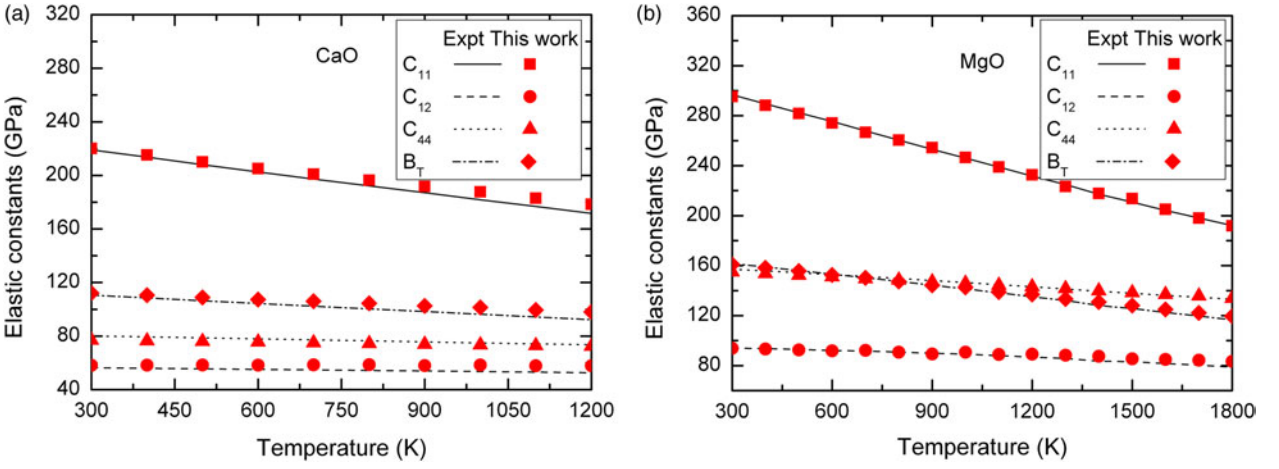

Figure 13. Temperature dependence of elastic constants for CaO and MgO.

introduced to heal the drawbacks arising from the sole pairwise potentials. The newly developed potentials for CaO and MgO are validated by a bundle of MD simulations on physical properties. Simulation results demonstrate the robustness of the developed interionic potentials.

In conclusion, we need to point out that the three-body interaction used in this paper only fits via elastic constants. We believe more physical properties included in the fitting process could lead to more accurate results, such as phonon dispersion and dielectric properties. In addition, more materials (e.g. Al_2O_3 or PbO_2) will be studied in future to extend the application of this approach. All these will be addressed in future studies.

Acknowledgements

This work was supported by the National Natural Science Foundation of China (10972066) and the Foundation of Excellent Youth of Heilongjiang Province. The authors would like to thank Dr Qingkun Li for helpful discussion.

References

[1] Zhang S, Chen NX. *Ab initio* interionic potentials for NaCl by multiple lattice inversion. Phys Rev B. 2002;66:64106-1–64106-10.
[2] Zhang S, Chen NX. Lattice inversion for interionic pair potentials. J Chem Phys. 2003;118:3974–3982.
[3] Wang C, Zhang S, Chen NX. *Ab initio* interionic potentials for CaO by multiple lattice inversion. J Alloys Compds. 2005;388:195–207.
[4] Ohta H, Hamaguchi S. Classical interatomic potentials for Si-O-F and Si-O-Cl systems. J Chem Phys. 2001;115:6679–6690.
[5] Ohta H, Iwakawa A, Eriguchi K, Ono K. An interatomic potential model for molecular dynamics simulation of silicon etching by Br(+)-containing plasmas. J Appl Phys. 2008;104:73302-1–73302-8.
[6] Cui ZW, Sun Y, Chen YJ, Qu JM. Semi-*ab initio* interionic potential for gadolinia-doped ceria. Solid State Ionics. 2011;187:8–18.
[7] Cui ZW, Sun Y, Qu JM. Molecular dynamics simulation of reduced CeO2. Solid State Ionics. 2012;226:24–29.
[8] Tsuchiya T, Kawamura J. Systematics of elasticity: *ab initio* study in B1-type alkaline earth oxides. J Chem Phys. 2001;114:10086–10093.
[9] Chang ZP, Graham EK. Elastic properties of oxides in the NaCl-structure. J Phys Chem Solids. 1977;38:1355–1362.
[10] Jeanloz R, Ahrens TJ, Mao HK, Bell PM. B1–B2 transition in calcium-oxide from shock-wave and diamond-cell experiments. Science. 1979;206:829–830.

[11] Karki BB, Stixrude L, Clark SJ, Warren MC, Ackland GJ, Crain J. Structure and elasticity of MgO at high pressure. Am Mineral. 1997;82:51–60.
[12] Karki BB, Wentzcovitch RM, de Gironcoli S, Baroni S. First-principles determination of elastic anisotropy and wave velocities of MgO at lower mantle conditions. Science. 1999;286:1705–1707.
[13] Hachemi A, Saoudi A, Louail L, Maouche D, Bouguerra A. Elasticity of the B2 phase and the effect of the B1–B2 phase transition on the elasticity of MgO. Phase Transitions. 2009;82:87–97.
[14] Mehl MJ, Hemley RJ, Boyer LL. Potential-induced breathing model for the elastic-moduli and high-pressure behavior of the cubic alkaline-earth oxides. Phys Rev B. 1986;33:8685–8696.
[15] Zhang H, Bukowinski MS. Modified potential-induced-breathing model of potentials between close-shell ions. Phys Rev B. 1991;44: 2495–2503.
[16] Matsui M. Breathing shell model in molecular dynamics simulation: application to MgO and CaO. J Chem Phys. 1998;108:3304–3309.
[17] Jahn S, Madden PA. Modeling earth materials from crustal to lower mantle conditions: a transferable set of interaction potentials for the CMAS system. Phys Earth Planet Int. 2007;162:129–139.
[18] Aguado A, Madden PA. Fully transferable interatomic potentials for large-scale computer simulations of simple metal oxides: application to MgO. Phys Rev B. 2004;70:245103-1–245103-6.
[19] Aguado A, Bernasconi L, Madden PA. Interionic potentials from *ab initio* molecular dynamics: the alkaline earth oxides CaO, SrO, and BaO. J Chem Phys. 2003;118:5704–5717.
[20] Wolf D, Keblinski P, Phillpot SR, Eggebrecht J. Exact method for the simulation of Coulombic systems by spherically truncated, pairwise $r(-1)$ summation. J Chem Phys. 1999;110:8254–8282.
[21] Clark SJ, Segall MD, Pickard CJ, Hasnip PJ, Probert MJ, Refson K, Payne MC. First principles methods using CASTEP. Z Krist. 2005;220:567–570.
[22] Frisch MJ, Trucks GW, Schlegel HB, Wallington, CT: Pittsburgh PA: Gaussian Inc.; 2003.
[23] Zhang S, Ph.D. Thesis (in Chinese), Tsinghua University ; 2002.
[24] Matsui M, Parker SC, Leslie M, The MD. simulation of the equation of state of MgO: application as a pressure calibration standard at high temperature and high pressure. Am Mineral. 2000;85:312–316.
[25] Jackson MD, Gordon RG. Electron-gas theory of some phases of magnesium-oxide. Phys Rev B. 1988;8:5654–5660.
[26] Marklund K, Mahmoud SA. Elastic constants of magnesium oxide. Phys Scr. 1971;3:75–76.
[27] Baltache H, Khenata R, Sahnoune M, Driss M, Abbar B, Bouhafs B. Full potential calculation of structural, electronic and elastic properties of alkaline earth oxides MgO, CaO and SrO. Phys B Condens Matter. 2004;344:334–342.
[28] Majewski JA, Vogl P. Crystal stability and structural transition pressures of Sp-bonded solids. Phys Rev Lett. 1986;57:1366–1369.
[29] Sims CE, Barrera GD, Allan NL. Thermodynamics and mechanism of the B1–B2 phase transition in group-I halides and group-II oxides. Phys Rev B. 1998;57:11164–11172.
[30] Liu ZJ, Sun XW, Ge SH, Wu HY, Zhang XL, Yang XD. Thermoelasticity of MgO at high pressures. Chin J Chem Phys. 2007;20:65–70.
[31] Louail L, Krachni O, Bouguerra A, Sahraoui FA. Effect of pressure on structural and elastic properties of alkaline-earth oxide CaO. Mater Lett. 2006;60:3153–3155.
[32] Karki BB, Ackland GJ, Crain J. Elastic instabilities in crystals from *ab initio* stress–strain relations. J Phys Condens Matter. 1997;9:8579–8589.
[33] Zha CS, Mao HK, Hemley RJ. Elasticity of MgO and a primary pressure scale to 55 GPa. Proc Natl Acad Sci. 2000;97: 13494–13499.
[34] Bond SD, Leimkuhler BJ, Laird BB. The Nose–Poincare method for constant temperature molecular dynamics. J Comput Phys. 1999;151:114–134.
[35] Souza I, Martins J. Metric tensor as the dynamical variable for variable-cell-shape molecular dynamics. Phys Rev B. 1997;55: 8733–8742.
[36] Sun G. Construction of high-order symplectic Runge-Kutta methods. J Comput Math. 1993;3:250–260.
[37] Cui ZW, Sun Y, Qu JM. The neighbor list algorithm for a parallelepiped box in molecular dynamics simulations. Chin Sci Bull. 2009;54:1463–1469.
[38] Anderson OL, Isaak DG. Mineral physics and crystallography: A. Handbook of physical constants. Washington, DC: American Geophysical Union; 1995.
[39] Fiquet G, Richet P, Montagmac G. High-temperature thermal expansion of lime, periclase, corundum and spinel. Phys Chem Miner. 1999;27:103–111.
[40] Cui Z, Sun Y, Li J, Qu J. Combination method for the calculation of elastic constants. Phys Rev B. 2007;75:214101-1–214101-6.